Eur. Phys. J. A (2011) **47**: 111
DOI 10.1140/epja/i2011-11111-7

THE EUROPEAN PHYSICAL JOURNAL A

Regular Article – Experimental Physics

Sub-barrier fusion of ^{6}He with ^{206}Pb

R. Wolski[1,a], I. Martel[2], Ł. Standyło[3,4], L. Acosta[2], J.L. Aguado[2], C. Angulo[5], R. Berjillos[2], J.P. Bolivar[2], J.A. Duenas[2], M.S. Golovkov[3], T. Keutgen[5], M. Mazzocco[6], A. Padilla[2], A.M. Sánchez-Benítez[2], C. Signorini[6], M. Romoli[7], and K. Rusek[4]

[1] Henryk Niewodniczański Institute of Nuclear Physics PAS, Cracow, Poland
[2] Departamento de Fisica Aplicada, Universidad de Huelva, E-21071 Huelva, Spain
[3] Flerov Laboratory of Nuclear Reaction, JINR, Dubna, Russia
[4] Andrzej Sołtan Institute for Nuclear Studies, Hoża 69, PL-00681, Warsaw, Poland
[5] Centre de Recherches du Cyclotron, Université Catholique de Louvain, B-1348 Louvain-la-Neuve, Belgium
[6] Dipartimento di Fisica and Istituto Nazionale di Fisica Nucleare, Sezione di Padova, I-35131, Padova, Italy
[7] Istituto Nazionale di Fisica Nucleare, Sezione di Napoli, Via Cintia, I-80126 Napoli, Italy

Received: 2 May 2011 / Revised: 2 September 2011
Published online: 23 September 2011

Communicated by N. Alamanos

Abstract. Cross-sections for the production of ^{210}Po nuclei in ^{6}He + ^{206}Pb collisions over the incident energy range 14–18 MeV were measured by means of the activation technique and a radiochemical analysis. The elastic scattering at 18.0 MeV was also measured providing a precise value for the ^{210}Po production cross-section at this energy. The results are at variance with the earlier experimental data and rather in accord with the predictions of a density-dependent barrier penetration model for the fusion process. A proper treatment of beam energy distribution for the evaluation of the activation data is discussed.

1 Introduction

Since the first experiments with light exotic nuclei twenty years ago, it has become clear that their specific structure can influence the interaction mechanism. In particular, the cross-section for the fusion of exotic nuclei at energies close to and below the Coulomb barrier could be strongly dependent on the projectile structure. The interest in this subject is evidenced by a series of reviews published in recent years: Liang and Siniorini [1] 2005, Canto *et al.* [2] 2006, Keeley *et al.* [3] 2009. From one point of view, an extended density distribution should favor the fusion probability. From another one, a weak binding energy could hinder it. Some models [2] predict a large increase in the fusion probability for exotic nuclei compared to that for ordinary nuclei. This effect is known as "sub-barrier fusion enhancement". Most experimental efforts to investigate such an effect have concentrated on ^{6}He beams due to their availability. However, there is a definition problem in the terminology used. The term "enhancement" implies the existence of a reference frame. The authors of [3] discuss two criteria to infer whether the fusion channel is enhanced or suppressed. One relies on comparing the fusion of the exotic nucleus to that for stable nuclei of similar mass with the same target. In the case of ^{6}He the comparison would be with data for ^{4}He. A straightforward comparison could be misleading because of the remarkable differences in mass and size. The second approach is to refer the fusion of the halo nucleus to the predictions of simple models generally established for the description of the fusion of stable nuclei. The One-Dimensional Barrier Penetration Model can serve this purpose with projectile density distributions explicitly taken into account. Another question is that the fusion of ^{6}He itself cannot be well defined experimentally either. The available ^{6}He beams have low intensities. Therefore, the fusion cross-section is usually determined from measurements of the induced radioactivity, either on-line for short-lived evaporation residues or off-line for long-lived ones, see, *e.g.*, the review [3] and references therein. The product of fusion followed by the evaporation of two neutrons is indistinguishable from a final nucleus produced by a direct α-particle transfer, see the discussion in [4]. The latter process is believed to be small at sub-barrier energies due to the presence of the Coulomb barrier, while the 1- or 2-neutron transfer processes could be large. The existing experimental data on ^{6}He sub-barrier fusion were reviewed in [1] and [3]. The authors concluded that the fusion enhancement, if present, is rather small [1,3] or absent [5].

Meanwhile, a large α-particle yield was observed in the ^{6}He + ^{209}Bi system at sub-barrier energies (see ref. [6] and references therein). This effect was also found later

[a] e-mail: wolski@nrmail.jinr.ru

Table 1. Production rate calculations for evaporation residues from ^{6}He + ^{206}Pb fusion reactions at projectile energies (MeV LAB) below and close to the barrier, in percentages.

^{6}He energy	^{211}Po	^{210}Po	^{209}Po	^{207}Pb
12.0	6.9	92.8		0.22
14.0	1.6	98.0		0.29
16.0	0.43	97.0	1.8	0.54
18.0	0.11	77.2	21.3	0.90
20.0	0.03	44.6	53.5	1.3

for other heavy targets [5]. The α-particle production at energies below the barrier is mostly due to neutron transfer, incomplete fusion and projectile breakup. It is known that the strength of such non-elastic processes depends on the projectile wave function and therefore could be a good tool to study the structure of halo nuclei. At sub-barrier energies, the cross-section for the α-particle channels almost reaches the limit of the total reaction cross-section, leaving little room for fusion, see refs. [5,6]. Therefore, the report [7] of a large sub-barrier fusion enhancement in the ^{6}He + ^{206}Pb scattering system was met with great interest. The fusion cross-section was measured by the stack activation technique. At beam energies close to and below the Coulomb barrier it is mainly the 2-n-evaporation channel that matters; other fusion-evaporation channels make minor contributions to the fusion. This is demonstrated by the results of Compound Nucleus evaporation calculations using the code EMPIRE [8] for the most prominent channels and several projectile energies in the range 12–20 MeV presented in table 1. The production rates for all energetically accessible evaporation residues were calculated. A large, updated data base for the spectroscopy of all the nuclei considered, *i.e.* the compound, intermediate and residual nuclei, was included in the calculations. It is interesting to see in table 1 small but nevertheless non-negligible contributions of the ^{207}Pb residue being a product of the α+n evaporation. In a real experiment, the same residue would be produced with much larger yield through the 1-neutron transfer reaction.

It is known that the code underestimates absolute values of the channel cross-sections due to unrealistic parameters for the ^{6}He entrance channel. However, it is believed that the calculations of the competition among the various evaporation channels are reliable. The accuracy of the results should be fairy high for the main channel and purely CN de-excitation if all the evaporation channels are included. A value of 3% for that accuracy was adopted. For extensive use of the code for non-equilibrium processes see ref. [9].

The data points reported [7] cover an energy region deeply below the barrier, never before attained in this kind of study. However, the rather large energy spread of the beam could make quantitative conclusions questionable. The authors explain their findings on the grounds of a model suggesting a sub-barrier sequential mechanism for fusion [10]. The model assumes that the fusion process proceeds through the $2n$ transfer to ^{208}Pb states as a first step. When low-lying states of the intermediate nucleus of large positive Q values are excited the released energy makes it easier for the α core to overcome the barrier. Thus a large gain in the fusion is obtained from a fraction of the $2n$ transfer strength corresponding to large Q values. Unfortunately, the model calculations for the $2n$ transfer process itself are not shown, making a confrontation with the existing data on neutron transfer reactions with ^{6}He projectiles [5,6,11] impossible. Based on the Q-value argument of the model an interesting implication can be drawn that the ^{6}He sub-barrier interaction could be dependent on the structure of the target nucleus. In particular, the sub-barrier fusion yield for the ^{6}He + ^{206}Pb system apparently should be larger than that for the ^{6}He + ^{208}Pb one. The authors of ref. [7] repeated their ^{6}He + ^{206}Pb fusion measurements with improved beam energy resolution [12]. The new results support the earlier findings. Some enhancement of sub-barrier fusion has recently been reported for the ^{8}He + ^{197}Au [13] and ^{9}Li + ^{208}Pb [14] systems. Nevertheless, the data for the ^{6}He + ^{206}Pb sub-barrier fusion show an exceptionally large enhancement much beyond the systematics for other systems presented in fig. 4 of ref. [12].

The aim of the present work was twofold. Firstly, it was needed to confirm the unexpectedly large fusion yield for the ^{6}He + ^{206}Pb system. Secondly, in a search for any target structure-dependent effect, high-quality data for the elastic and inelastic scattering processes had to be obtained and compared with the existing data for the ^{6}He + ^{208}Pb reaction [11]. The idea was to activate the ^{206}Pb material and measure the elastic and inelastic products in a single experimental run. Moreover, the fusion cross-section for the ^{206}Pb scattering target could be determined highly accurately due to the normalization of the forward-angle elastic-scattering cross-section to the Rutherford value. The fusion of ^{6}He followed by the evaporation of two neutrons induces ^{210}Po α-radioactivity which had to be measured off line. The experiment is described below and the results for the fusion are presented. The complete analysis of the scattering data will be published separately [15].

2 Experiment and analysis

The experiment was carried out at the Centre de Recherches du Cyclotron at Louvain-la-Neuve (Belgium) where a ^{6}He radioactive beam was obtained by the ISOL method. The first report on a short-lived radioactive ion beam produced by this method of using two accelerators can be found in [16]. The ^{6}He was produced through the ^{7}Li$(p,2p)^{6}$He reaction by bombarding a powder LiF production target with a high current 30 MeV proton beam. The ^{6}He atoms were extracted, transferred to the ion source, ionized to the ^{6}He^{+} state, and accelerated to 18.0 MeV with an energy resolution not exceeding 90 keV FWHM ($\sigma = 38.2$ keV). The beam intensity was up to 10^{7} particles per second and free of any detectable contaminants. The ^{6}He^{+} beam was focused on a scattering target

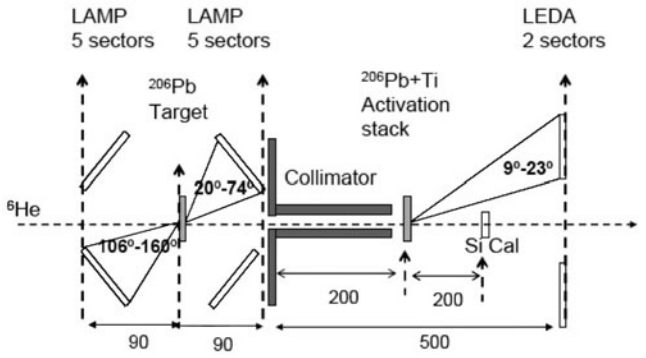

Fig. 1. Experimental setup for two independent measurements: scattering of 18.0 MeV ^{6}He beam on a ^{206}Pb target measured by 2 LAMP detectors and the activation of the stack of foils by passing ^{6}He ions monitored by 2 LEDA sectors. The collimator shield separates the two parts of the scattering chamber. The SiCal detector was inserted in the beam for a calibration run only. All dimensions are in mm. See text.

localized inside a scattering chamber, see fig. 1 for the experimental setup. The beam spot was not measured in the present experiment but, according to earlier studies at this facility with this scattering chamber, should be of 5–7 mm in diameter. Subsequently, the beam passed through a collimator, a stack of activation foils and was finally stopped in a Faraday cup. The collimator had entrance and exit baffles of 10 mm in diameter and was mounted on a shield that separated the scattering chamber into two parts, the first dedicated to the scattering experiment and the activation of the scattering target and the second to the stack activation. A Faraday cup current meter served for tuning the machine and to control beam stability. The absolute intensity measurements were done by other methods, independently for the scattering measurement and the activation of the stack of foils.

The collimator with additional shielding was used to prevent charged products back-scattered from the stack hitting the detectors in the first part of the chamber. All targets were made as foils and fixed to rectangular frames of 15 mm central aperture. Two different types of target were used in the present experiment. Targets of Type I were a layer of enriched ($> 97\%$) ^{206}Pb metal of (0.50 ± 0.05) mg/cm^2 thickness evaporated on a 40 μg/cm^2 thin Carbon foil. According to TRIM calculation the thickness of the Carbon backing was sufficient to stop the fusion produced ^{210}Po evaporation residues. Targets of Type II were made by depositing a disk-shaped layer (15 mm diameter) of ^{206}PbS compound on 1.5 μm thick Ti foils. The material used was of enrichment $> 95\%$, the rest being ^{207}Pb and a small amount ($< 1\%$) of ^{208}Pb. The ^{210}Po nuclei of interest can be produced by the interaction of the ^{6}He beam with ^{207}Pb material through the fusion+3n evaporation reaction. The cross-section for this process is 40%, 24% and 11% of the fusion at 18.0, 17.0, 16.0 MeV, respectively. Therefore, the ^{207}Pb contamination in the targets introduced small contributions to the ^{210}Po activity. The last stack Type II target had a 2.0 μm Ti foil as a backing. The Ti foils served as beam energy degraders. An electro-chemical method was used to manufacture these targets in teflon cylindrical vessels of 15 mm diameter. The method, tested with natural Pb, is able to produce homogeneous layers up to 600 μg/cm^2 in thickness. Since our intention was to use thicker targets in order to increase the sensitivity of the fusion measurements we ignored that limit and obtained a larger average thickness of the ^{206}PbS compound in Type II targets at the possible expense of uniformity. The thicknesses were estimated by weighing to be around 1 mg/cm^2 and, in fact, a check done with an α source revealed local heterogeneities of the compound thickness in the target spot. In any case the total foil stack thickness was measured during the experiment.

The scattering target and the first target of the activation stack were Type I targets. This was done to check the consistency of the independent induced radioactivity measurements in the scattering experiment and in the irradiation of the foils. The rest of the activation stack was made of a 1.5 μm Ti foil as the first ^{6}He energy degrader followed by 8 Type II targets mounted in 4 pairs each of face-to-face pieces to make the effective targets thicker and to smear somewhat the individual target heterogeneity. Thereby beam energy losses in the activated material were close to those in Ti degraders.

It is known that ^{210}Po is present in the environment as a product of the ^{238}U decay chain. Therefore two Type II targets were installed on a stack ladder inside the scattering chamber but beyond the beam line for off-line determination of the background.

Charged particles emitted by the scattering target were detected by the large area Si multi-detector system LEDA (Louvain Edinburgh Detector Array) [17]. One LEDA array is an annular detector consisting of 8 sectors, each having 16 strips of 10.0 mm width. The removal of two sectors from the complete detector enables the remaining sectors to be arranged as a six-sided cone —colloquially know as the "lamp configuration". This configuration has the advantage of providing very large solid angles but at the expense of a rather complicated geometry and a poorer angular resolution [17]. Forward and backward scattering angles were covered by 2 LAMP sets of 5 LEDA sectors each. The elastic scattering of ^{6}He on ^{206}Pb was identified in the energy spectra of all strips as a sharp peak. It was assumed that, apart from the elastically scattered ^{6}He nuclei, only α-particles originating from transfer and breakup could be detected. They were seen as broad maxima with average energies close to that of the elastic scattering.

Two additional LEDA sectors were mounted downstream of the stack for measuring the total flux of projectiles activating the foil stack.

The energy deposition in the detectors and the time with respect to the Cyclotron RF were collected by an acquisition system in the total "OR" regime. The dead time was of the order of 8–10% on average for the main run, including beam-on but acquisition-off intervals.

In order to calibrate the counting rates of the LEDA monitor strips with respect to the projectile flux passing through the stack as well as to measure the stack total

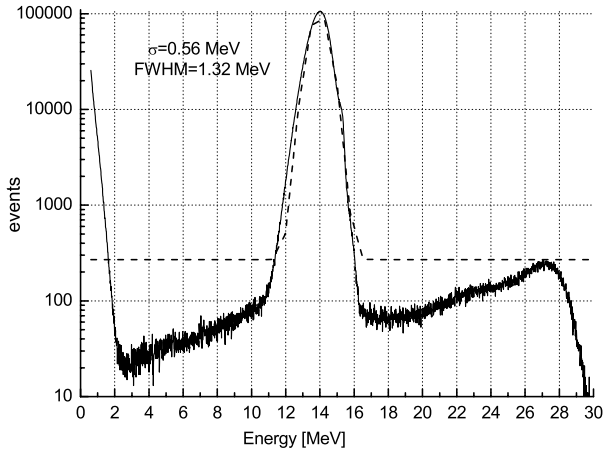

Fig. 2. The energy distribution of the beam passed through the activation stack measured by SiCal detector during a calibration run. The dashed line is a Gaussian approximation with $E_{max} = 13.95\,\mathrm{MeV}$ and $\sigma = 0.56\,\mathrm{MeV}$.

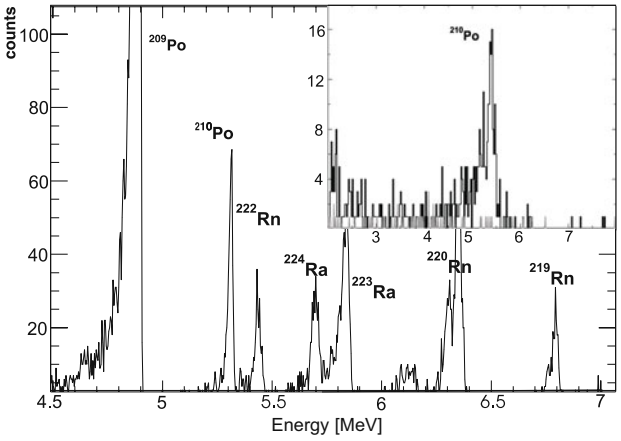

Fig. 3. Alpha-particle energy spectrum for a Type II target activated at 15.6 MeV ^{6}He beam energy and measured during 23 d, 480 and 6299 decay events were registered for ^{210}Po and ^{209}Po, respectively, see text for more details. The inset shows the α-particle spectrum adapted from ref. [12] corresponding to 15.3 MeV bombarding energy.

energy loss and its final energy distribution a special calibration run was performed. For this run with a very low intensity beam a dedicated Si detector, (SiCal) in fig. 1, was inserted in the beam line downstream of the stack. During the main experiment this detector was removed from the beam. The detector itself was energy calibrated prior to and after the experiment by a standard triple α-line source.

The beam energy distribution measured in the calibration run is shown in fig. 2. Beneath the main peak a broad structure is seen. Its contribution is 1.64% of the total number of detected events. This is consistent with pileup for the particle load on the (SiCal) detector, $(7\text{–}8)\cdot 10^3\,\mathrm{s}^{-1}$ and its shaping time of 2μs. The energy spectrum in fig. 2 demonstrates the energy loss in the stack and a large energy spread. The energy loss is apparently 0.47 MeV larger than the value estimated by TRIM using the nominal thicknesses of the Type II targets. In order to match the experimental stack energy loss we had to assume that the ^{206}PbS target material is 27% thicker than initially estimated by weighing. The thickness of selected Ti backing (degrading) foils was measured by an α-source and found to be in agreement with the the nominal values of 1.5 μm or 2.0 μm. Perhaps the ^{206}PbS layers had more material in the central, active area of the targets than at the edges of the target material disk. The uncertainty in the material density for individual pairs of two Type II targets was safely taken to be $\pm$10%. The possible effect of the beam energy dispersion on the cross-section measurements is discussed below.

In order to measure induced ^{210}Po α-activity all irradiated targets as well as the Ti degrader foil and one of the non-irradiated targets were processed at the Radiochemical Laboratory of the University of Huelva which performs such studies on a routine basis [18]. A method of traced atoms had been applied there [19,20]. Each foil was dissolved in *aqua regia* and around of 17 mBq of ^{209}Po added as a tracer to monitor the efficiency of an involved chemical process [21]. Tracer portions were obtained from an original capsule provided by a manufacturer and certificated by NIST as having a ^{209}Po specific activity of 85.83 Bq/g. The required metallic fraction was extracted and put into dedicated α-activity measurement cells, each equipped with 450 mm^2 ORTEC silicon detectors of energy resolution less than 20 keV for the ^{241}Am line and subtending 0.25 of the full solid angle for an ideal source. Since the half-life of the ^{210}Po α-decay is 138.38 d, the activity measurements lasted up to 25 d depending on sample counting rates. The background of ^{210}Po activity for the empty cells was routinely measured in advance. All energy spectra clearly exhibit the presence of the α-particle energy at 5.3 MeV from the decay of ^{210}Po and the tracer α-line. An example of the α-particle energy spectrum for a target sample activated at 15.6 MeV projectile energy is given in fig. 3. The spectrum was measured over 23 d and 480 ^{210}Po and 6299 ^{209}Po decay events were recorded in total. During 9.5 d of a pertinent background measurement 60 events were collected. The total relative error for this activity measurement was estimated to be 12%. Others α-particle energy lines seen in fig. 3 have been identified by ref. [22]. An inset in fig. 3 shows α-particle spectrum obtained earlier for a target activated at 15.3 MeV [12]. The total effectiveness, including a geometrical one, for the tracer detection varied from 0.03 up to 0.2. The accuracy of the α-activity measurements was estimated to be from 6.5% for the scattering target sample up to 25% for a sample of the lowest detection efficiency. Apart from the statistical errors the inaccuracy of the tracer dropping procedure contributes to these errors. Possible losses of ^{210}Po atoms, due to its volatility, in a period prior to the chemical processing, were neglected.

To determine the reaction cross-section of interest, σ_{2n}, the product of the total integrated projectile flux bombarding the scattering target and its density was obtained by normalizing the elastic scattering count rate to Rutherford scattering.

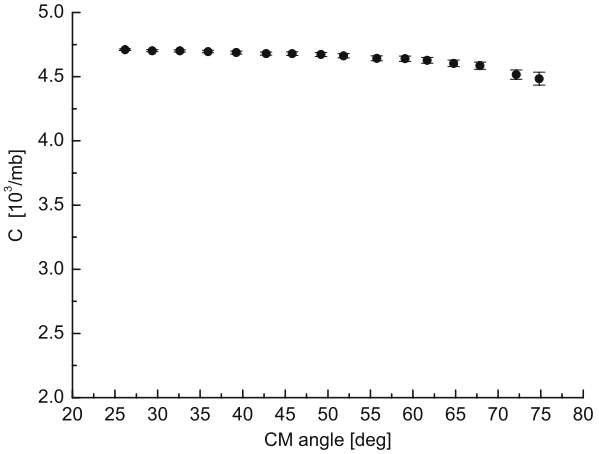

Fig. 4. The elastic-scattering angular distribution, normalized with the constant C, measured by 5 sectors of the forward angle LAMP detector and corrected according to [23], see text.

Let N_i be the number of elastic scattering events recorded in a solid angle $\Delta\Omega_i$ subtending the scattering angles θ_i,

$$N_i = C \int_{\Delta\Omega_i} \left(\frac{\mathrm{d}\sigma(\theta_i)}{\mathrm{d}\Omega} \right)_{el} \mathrm{d}\Omega, \qquad (1)$$

where C, in units of $1/\mathrm{cm}^2$, is the product of the scattering target density and the integrated incoming particle flux.

$\left(\frac{\mathrm{d}\sigma(\theta)}{\mathrm{d}\Omega}\right)_{el}$ is the elastic scattering cross-section described at forward angles by the Rutherford formula. At the same time the number of activated nuclei in the scattering target, N_a, is given by:

$$N_a = C \cdot \sigma_{2n}, \qquad (2)$$

where σ_{2n} is the cross-section for the $2n$ evaporation channel.

Because of the compact geometry of the LAMP detector configuration the values of the scattering angle θ_i and solid angle $\Delta\Omega_i$ were quite sensitive to non-ideal beam optics. Therefore, the constant C was not the same for all detector strips covering the angular range where the Rutherford formula is valid. Two different software procedures were applied to optimize the measured elastic scattering angular distributions at forward scattering angles. The first was borrowed from [23]. It is assumed there that the deviation of the measured angular distribution from that of Rutherford scattering is due to the beam misalignment contribution to the change in the scattering angle subtended by each strip [23]. The outcome of an optimization of the beam axis angle with respect to that of the scattering chamber is shown in fig. 4. Taking into account only 8 data points corresponding to polar angles $< 50^\circ$ a value for $C = 4.69 \cdot 10^3 \frac{1}{mb}$ was obtained. In the second treatment the unmeasured beam spot diameter and eccentricity of the beam axis from the center in the target plane were varied to tune the polar and solid angles of all strips. The former variable was of small impact on the angular distributions. The detector-target distance was also varied within the limits of the supporting mechanical construction accuracy. The second procedure provided an average value of $C = (4.83 \pm 0.037) \cdot 10^3 \frac{1}{mb}$ for the 8 most forward angles of all sectors. The average of these two values was taken for the constant $C = 4.76 \cdot 10^3 \frac{1}{mb} \pm 3\%$.

Having determined the constant C and the number N_a provided by the measured α-radioactivity the cross-section of interest for the scattering target, σ_{2n}, is given by eq. (2) and corrected for the dead time.

The integrated projectile flux entering the activation stack was given by the LEDA strips monitor count rates scaled by constants measured in the calibration run. This measurement is independent of the efficiency factor for the beam transmission through the collimator, which was below 50% in average.

The induced radioactivity data have to be corrected for the natural radioactivity background. The measurement of the background target sample yielded a value which corresponds, under the conditions of the present experiment, to a background of $1.5\,\mathrm{mb} \pm 24\%$ in the σ_{2n} measurements for the activated material in the Type II targets. An α-radioactivity value for the Ti foil sample was of 40% that for the background target sample. That level of the background contributes considerable to overall accuracy of the measured cross-section at low energies.

The background corrected σ_{2n} data provided by the experiment are shown in fig. 5 together with the earlier data [12] digitalized and the predictions of the sequential fusion model [7,10]. It is notable that our 2 data points at laboratory energies close to 18.0 MeV obtained by different methods are self-consistent. We note that the present experimental points are in disagreement with the earlier data [7,12] and do not follow the predictions of the sequential fusion model [10], represented by the dotted line in fig. 5.

One could expect an overestimation of the measured data due to the finite energy spread of the beam traversing the stack materials. The effect produced by the beam energy distribution for each pair of targets is discussed below.

2.1 Energy averaging correction

Any measurement of an energy-dependent cross-section made with a beam of finite energy dispersion results in data points averaged over a finite energy range. For a weakly energy-dependent quantity the averaging is unimportant. However, the fusion cross-section at sub-barrier energies can be approximated by $\exp(\frac{E}{\omega})$, where $\frac{1}{\omega}$ is the logarithmic slope of the function. Such a strong energy dependence is characteristic of the barrier penetration probability, as can be seen in fig. 5 and in fig. 6 for the two model calculations, and even the $\frac{1}{\omega}$ coefficients are very similar for these entirely different theoretical approaches. Another energy-dependent function needed here is the beam energy distribution. The final ^{6}He beam energy distribution was fairly well approximated by a Gaussian, $\exp(-\frac{E^2}{2\sigma_E{}^2})$, with a FWHM = 1.32 MeV

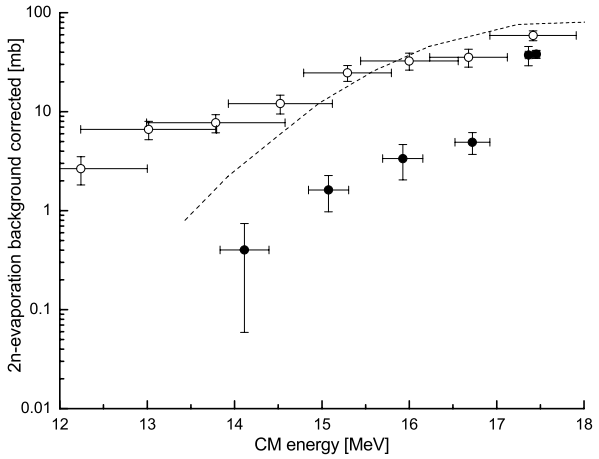

Fig. 5. Data for ^{210}Po production in the interaction of ^{6}He with ^{206}Pb for projectile energies below 18 MeV LAB. Open symbols denote digitalized data from [12], solid circles for the background corrected data of the present experiment, two data points at the highest energies were obtained for thin targets by different methods, horizontal bars indicate energy losses in the targets only, the data are uncorrected for beam energy spread, see text. The dashed curve is the prediction of the sequential fusion model for the $2n$ evaporation channel [7,10].

($\sigma_E = 0.56$ MeV), see fig. 2. Such a large final σ_E is caused mainly by the heterogeneity of the stack thickness.

Taking the defined beam energy distribution and the exponential dependence of the studied cross-section, one has to find an effective energy for each data point and shift the point towards a higher energy from the energy value calculated for the middle of the target layer. The corresponding values of this shift E_{shift} were given by the averaging procedure

$$E_{shift} = \frac{\int_{-\infty}^{\infty} E \exp\left(-\frac{E^2}{2{\sigma_E}^2}\right) \exp\left(\frac{E}{\omega}\right) \mathrm{d}E}{\int_{-\infty}^{\infty} \exp\left(-\frac{E^2}{2{\sigma_E}^2}\right) \exp\left(\frac{E}{\omega}\right) \mathrm{d}E} = \frac{\sigma_E^2}{\omega}. \quad (3)$$

The integrals in eq. (3) are calculable analytically [24]. One can see from eq. (3) that even for a thin target the energy coordinate for the given data point is not the most probable energy in the target middle, but is shifted from this value upward by an amount E_{shift}. The effect can be large for $\sigma_E > \omega$.

For a thick target one also has to make an additional averaging over the target thickness. Let us take ΔE for the energy loss in a homogeneous target. The beam energy dispersion is not a constant within the target. It increases with decreasing energy. Due to the statistical nature of the energy loss mechanism, a linear energy dependence can be postulated:

$$\sigma_E(E)^2 = \sigma_0^2 - aE,$$

where σ_0^2 is for the target middle, and a is a linear coefficient.

Under assumption that the coefficient a is constant for the stack its value can be estimated from the initial energy dispersion $\sigma(E_{in}) = 0.038$ MeV, the final one $\sigma(E_{fin}) = 0.56$ MeV and the total energy loss $\Delta E_t = 4.0$ MeV

$$a = (\sigma(E_{fin})^2 - \sigma(E_{in})^2)/(4.0\,\mathrm{MeV}) = 0.078\,\mathrm{MeV}.$$

Thus the target-thickness weighted energy shift is

$$\langle E_{shift} \rangle = \frac{\int_{-\Delta E/2}^{\Delta E/2} \sigma^2(E) \exp\left(\frac{E}{\omega}\right) \mathrm{d}E}{\omega \int_{-\Delta E/2}^{\Delta E/2} \exp\left(\frac{E}{\omega}\right) \mathrm{d}E} = \frac{\sigma_0^2 - \frac{a}{2\omega}\left(\frac{\Delta E}{2}\right)^2}{\omega}. \quad (4)$$

The right side of eq. (4) is the result of the second-order exponential expansion. Having in mind the derived formulas, the energy corrections in question can be evaluated. The fusion cross-section slope parameter $\omega = 0.58$ MeV was taken from the barrier penetration model calculations shown in fig. 6. This reasonable assumption makes the treatment somewhat model dependent. However, ω is almost energy independent for a given target at energies below the barrier, see the straight line for the fusion cross-section in figs. 5 and 6. This value is close to the dispersion parameter σ_E for the last foil in the activation stack. Therefore, for the lowest energy the maximal energy shift upward, E_{shift}, is equal to 0.47 MeV CM. The second-order correction described by the second term in eq. (4) is insignificant for the present data. However, if the energy averaging procedure given by eq. (3) is disregarded the corresponding cross-section becomes overestimated by a factor of 3. The situation rapidly deteriorates with the broadening of the ^{6}He beam energy distribution. For example, an overestimation by one order of magnitude would be apparent for a beam energy distribution of FWHM = 2.0 MeV.

The relevant dispersion parameters of the energy distribution were calculated for each target pair according to the linear dependence of $\sigma(E)^2$ on the beam energy and the resulting energy corrections imposed. The final results for the ^{6}He + ^{206}Pb fusion calculated from the $2n$ evaporation data are shown in fig. 6 as closed dots. The horizontal bars on these data points represent the beam energy loss in a given target. For the Type I targets, which are thin and where the beam is rather monochromatic, the corrections are negligible.

The corrected experimental data are not in large disagreement with the calculations of the barrier penetration model (BPM), shown as the solid line in fig. 6. The model seems to be an accepted description for light particle fusion at energies close to and below the barrier [3]. In this model a sum of the combined Coulomb plus nuclear potentials could be approximated by an inverted parabola and the Hill-Wheeler formula applied for the barrier penetration probability. The nuclear potential used here is of double-folding type with the ^{6}He density taken from [25] providing a barrier height of 18.6 MeV. The sensitivity of the calculated fusion cross-section to the various density parameterizations is discussed in ref. [3].

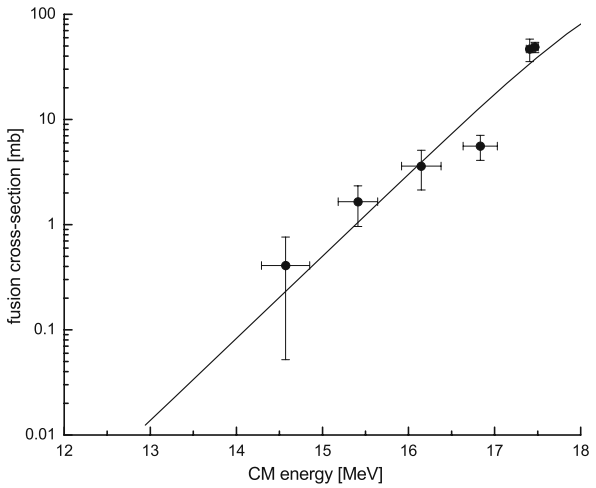

Fig. 6. The present experiment data for the ^{6}He + ^{206}Pb fusion cross-section. Symbols for the experimental data corrected for the beam energy distribution, horizontal bars for energy losses in the targets only, vertical bars correspond to combined errors of α-activity, target thickness, integrated beam flux or constant C measurements, background subtraction and statistical model calculations. The curve denotes the double-folding barrier penetration calculation with the Coulomb barrier equal 18.6 MeV, see text.

3 Conclusions and remarks

The cross-sections for the production of ^{210}Po nuclei in the interaction of ^{6}He projectiles with a ^{206}Pb target were measured down to a level few hundreds of μb and below the natural radioactivity background. The stack activation method was used for this purpose followed by off-line radiochemical analysis. The measurement was performed in the energy region 14–18 MeV, definitely below the Coulomb barrier. In the same experimental run the elastic scattering and α-particle production cross-sections were measured at an energy of 18.0 MeV LAB. The data were collected by means of the large area multi-detector system LEDA. The elastic scattering served for the absolute normalization of the activation data for the highest energy of 18.0 MeV providing a high-precision value for the cross-section at that energy. The data obtained from the stack activation technique were subjected to an analysis aimed to investigate an influence of the finite beam energy spreading on the measured cross-sections. Analytical formulas were derived, based on simple approximations, to estimate the effect which is sometimes left out. This correction appeared to be rather significant if the beam energy dispersion is comparable to or larger than the exponential slope parameter of the fusion cross-section energy dependence. For that reason the earlier fusion data obtained by the activation method with beams of large energy spreading could be inconclusive.

The 2-neutron evaporation channel practically exhausts the total fusion cross-section in the reaction studied, except at the highest energies available in the present experiment. The experimental fusion data points are rather close to calculations made using the one-dimensional barrier penetration model with a microscopic density distribution for ^{6}He, if one neglects a possible enhancement at 17.5 MeV CM and ignores an apparent disagreement at 17 MeV. Within an accuracy attained any dramatic enhancement of the ^{6}He fusion for energies deeply under the barrier was not observed. It is not excluded that such effects could be present at yet lower energies. Therefore, an effort would be desirable to improve the beam energy resolution at these energies what is quite instrumental for measurements of a strongly energy dependent cross-section. However, a dedicated experiment would be rather difficult for the present projectile + target combination because the cross-sections of interest would be generally close and below of the natural ^{210}Po background level. Maybe other techniques, on-line spectroscopy for example, would be more suitable for future intense exotic beams studies. A powerful method of that kind has been already demonstrated in off and on-line fusion and reaction channels cross-section measurements using rather low-beam intensities [13,26].

The authors would like to thank A. Daniel for EMPIRE calculations, R. Raabe for providing the barrier penetration model numerical data, Yu.Ts. Oganessian for his interest and illuminating discussions, N. Keeley for reading the manuscript, G. Ryckewaert and M. Loiselet for an excellent beam performance and M. Loriggiola for manufacturing Type I targets.

References

1. J.F. Liang, C. Signorini, Int. J. Mod. Phys. E **14**, 1121 (2005).
2. L.F. Canto *et al.*, Pys. Rep. **424**, 1 (2006).
3. N. Keeley, R. Raabe, N. Alamanos, J.L. Sida, Prog. Part. Nucl. Phys. **63**, 396 (2009).
4. A. Navin *et al.*, Phys. Rev. C **70**, 044601 (2004).
5. R. Raabe *et al.*, Nature (London) **431**, 823 (2004).
6. J.J. Kolata, Eur. Phys. J. A **13**, 117 (2002).
7. Yu.E. Penionzhkevich, V.I. Zagrebaev, S.M. Lukyanov, R. Kolpakchieva, Phys. Rev. Lett. **96**, 162701 (2006).
8. M. Herman, Nucl. Data Sheets **108**, 2655 (2007).
9. C. Kalbach, Phys. Rev. C **71**, 034606 (2005).
10. V.I. Zagrebaev, Phys. Rev. C **67**, 061601 (2003).
11. D. Escrig *et al.*, Nucl. Phys. A **792**, 2 (2007).
12. S.M. Lukyanov *et al.*, Phys. Lett. B **670**, 321 (2009).
13. A. Lemasson *et al.*, Phys. Rev. Lett. **103**, 232701 (2009).
14. A.M. Vinodkumar *et al.*, Phys. Rev. C **80**, 054609 (2009).
15. Ł. Standyło *et al.*, in preparation.
16. D. Darquennes *et al.*, Phys. Rev. C **42**, 804 (1990).
17. T. Davinson *et al.*, Nucl. Instrum. Methods A **454**, 350 (2000).
18. R.L. Lozano *et al.*, to be published in Nucl. Instrum. Methods A (2011), doi: 10.1016/j.nima.2011.08.006.

19. F. Flynn, Anal. Chem. Acta **43**, 221 (1968).
20. E. Holm, R. Fukai, Talanta **24**, 659 (1977).
21. Analyt. Quality in Nucl. Appl. No. IAEA/AQ/12 (2009).
22. J.B. Marion, F.C. Young, *Nuclear Reaction Analysis; Graph and Tables* (North-Holland Publishing Company, Amsterdam, 1968) p. 143.
23. J. Rahighi *et al.*, Nucl. Instrum. Methods A **578**, 185 (2007).
24. I.M. Ryzyk, I.S. Gradsztein, *Tables of Integrals, Sums, Series and Products* (PWN, Warszawa, 1964) p. 171.
25. I. Tanihata *et al.*, Phys. Lett. B **289**, 261 (1992).
26. A. Lemasson *et al.*, Phys. Rev. C **82**, 044617 (2010).